Research Paper

Numerical investigation of a CO_2 cooling system connected to Spawn-of-energy-plus thermal zones

Hagar Elarga [a,*], Håkon Selvnes [b], Alexis Sevault [b], Armin Hafner [a]

[a] Energy and Process Technology Department, Norwegian University of Science and Technology, Kolbjørn Hejes vei 1D, 7491 Trondheim, Norway
[b] SINTEF Energy Research, 7465 Trondheim, Norway

ARTICLE INFO

ABSTRACT

Today, only about 25 % of the European building stock is considered energy efficient. Meanwhile, the implementation of CO_2 as a refrigerant is considered one of the solutions to improve the overall building's energy performance, especially if the heat recovery concept is applied. In the current study, a detailed dynamic simulation model of a CO_2 chiller connected to the American Department of Energy reference small office building represented via Spawn-of-EnergyPlus is investigated for three different weather conditions in Chicago, Oslo, and Athens and two scenarios with heat recovery and without heat recovery. Three Modelica libraries of the thermal systems from TLK-Thermo GmbH, Modelica standards, and Modelica Buildings were used to develop the models. The simulation was executed on Modelica/Dymola simulation platform, and it lasted for five days. Results demonstrated that in the scenario with heat recovery, the system COPs are improved to 4.9, 5.4, and 7.2 from 2.2, 2.9, and 5.3 for Athens, Chicago, and Oslo, respectively.

1. Introduction

1.1. Clean refrigerant CO_2 (R744)

A large part of the energy used in the European building stock goes to waste, and such energy loss can be minimized by improving existing buildings and striving for innovative solutions [1]. On the other hand, spreading the technology use of CO_2 (R744) and other natural working fluids as a refrigerant have become a worldwide obligation due to the rising negative impacts of global warming and also due to the environmental concerns of synthetic refrigerants [2]. Compared to other natural refrigerants, CO_2 is unique because it is neither flammable nor toxic [3]. It has an Ozone depletion of zero and has a shallow direct impact on global warming. R744 has other benefits compared to HFC systems, such as a high volumetric refrigeration capacity (four to ten times) and the required volume stroke in the compressor being consequently low [4]. However, the main characteristic that separates CO_2 from the other refrigerants is the low temperature of the critical point (31.0 °C) and high pressure (73.8 bar). The low critical temperature indicates that the practical upper level for achieving condensation inside a condenser/gas cooler is around (28C) [5]. In other words, the heat rejection process of the refrigeration/cooling cycle needs to be performed in the transcritical region at ambient temperatures close to or above the critical temperature [5].

On the other hand, the large temperature glide in the gas cooler results from the isobaric heat emission above the critical point[6] makes R744 (CO_2) an efficient refrigerant for heating and Domestic Hot Water DHW applications compared to HFC-based systems.

1.2. Cooling, Heating, and refrigeration applications of CO_2(R744)

CO_2 thermal systems could be utilized in various applications, which opens the research door to investigate several design aspects. Luo et al. [7] performed an experimental investigation on the performance of a single-stage compound air source heat pump using CO_2/R600 under different operating conditions. The results showed that the system coefficient of performance (COP) varied from 1.834 to 2.574 when air inlet temperature varied from −30℃ to 0℃, and the thermodynamic perfection of the compound heat pump cycle was higher than 46 % in the experiment. Cui et al.[8] highlighted that the pinch point in the gas cooler significantly impacts the optimal discharge pressure and system performance of the CO_2 heat pump water heater. For that, a thermodynamic model was developed and validated, and a faster and more effective method for seeking optimal discharge pressure was proposed and proven accurate.

Nomenclature

A_{eff}	The valve cross-sectional area $[m^2]$
c_w	Water-specific heat capacity [kJ kg^{-1} K^{-1}]
EntFlowSpawn	The summation of the enthalpy flows connected through SPAWN fluid ports [W]
h_{flow}	The enthalpy of the airflow [J kg^{-1}]
HP_{set}	High pressure side setpoint value [bar]
$\overset{\circ}{m}_{air}$	The summation of the airflow rate of all fluid ports connected to the SPAWN component, i.e. entering (positive sign) and leaving (negative sign), i.e. according to the Modelica conventions. [kgs^{-1}]
$\dot{m}_{heaW}$	Heating water flow rate [kg s^{-1}]
$\dot{m}_{ref}$	Refrigerant mass flow rate [kg s^{-1}]
$p_{SucReset}$	The setpoint suction pressure [bar]
P_{gcFan}	Gas cooler fan shaft power [W]
P_{Com}	Compressor shaft power [W]
Δp	The pressure gradient across the valve [Pa]
Q_{total}	The summation of exchanged sensible and latent heat flow between EnergyPlus and Modelica sides [W]
Q_{Eva}	Evaporator heat flow [W]
Q_{HR}	Heat recovery heat flow [W]
RH	Relative Humidity [%]
SH	Super Heating [K]
$T_{heaWOutlet}$	Heating water leaving the heat recover heat exchanger [K]
$T_{heaWInlet}$	Heating water entering the heat recovery heat exchanger [K]
T_{Air}	Thermal zone measured air temperature [C]
U	The system's internal energy or the air heat storage energy [J]

Subscript

AppAbs	Approach Absolute

ambDB	Ambient dry bulb
Com	Compressor
Eva	Evaporator
Eff	Effective area
gc	Gas cooler
gcout	Refrigerant leaving the gas cooler
heaW	Heating water
i	Start of the simulation time
Q_{HR}	Heat recovery heat flow
ref	Refrigerant
SucReset	Suction Reset
W	Water

Greek symbols

ρ_{in}	the inlet flow density [kg m^{-3}]

Abbreviations

conFC	Constant frequency compressor
COP	Coeffcient of performance
DHW	Domestic Hot Water
DOE	Department of Energy-US
DX	Direct exchange
EnOB	An eco blog with a clear purpose
GC	Gas Cooler
GHC	Greenhouse Gas
HP	High Pressure
HVAC	Heating Ventilation Air Conditioning
PID	Piping and instruments diagram
PI	Proportional Integral controller
RIHC	Refrigeration Integrated Heating and Cooling
varFC	Variable frequency compressor
WHR	With Heat Recovery
WOHR	Without Heat Recovery

In addition to all its environmental gains, R744 could be promoted as a single-unit refrigerant, meaning it can simultaneously meet the required building refrigeration cooling and heating requirements [9].

One of the first examples of such a single unit system was implemented at the EnOB [10] project, where the unit provided commercial cooling for the chiller cabinet and freezers in the sales area and the cold stores in the storage area as well as space heating/cooling and pre-heating/cooling of the ventilation air [11]. Minetto et al. [12] described the development of a reversible heat pump for space heating and cooling based on a CO_2 transcritical cycle, which aims to recover the expansion work loss using a two-phase ejector. The experimental assessment of the heating and cooling mode operations was reported to maintain satisfactory values for COP and energy efficiency ratio under the capacity of the proposed layout to operate as a heat pump and chiller.

1.3. CO_2 thermal system modelling

Modeling of CO_2 systems has proved a remarkable capability for investigating some innovative systems and ideas.

Maouris et al. [13] have investigated numerically the performance of an integrated CO_2 refrigeration integrated heating and cooling RIHC system with thermal storage. Results have shown that adopting a RIHC system with thermal storage can decrease the annual greenhouse gas GHG emissions and energy consumption by 13 % and 18 %, respectively, compared to a conventional heat recovery plus gas boiler solution.

A comparative numerical analysis between the implementation of the vapor ejector and high-pressure valve showed an increase in the global system efficiency by 15 % for the first case system [14]. Operating challenges, such as controlling the high-pressure valve for a CO_2 refrigeration system integrated with AC production, were discussed [15]. The solution included a control strategy based on setting the AC evaporation pressure, calculating the ideal pressure lift for the AC ejector at those ambient conditions, and using it to determine the set-point for the control of parallel compressors. Sawalha [16] developed a numerical model to assess the performance of a commercial CO_2 transcritical booster system for refrigeration and heating of an average supermarket in Sweden. The results have shown that thermal energy usage of the supermarket would be slightly reduced if a CO_2 booster system with heat recovery was used instead of conventional solutions.

Jin et al. [17] developed a quasi-steady state and transient models for a single vapor compression cycle for independent cooling and dehumidification of indoor air conditioning systems. It was shown that the two-phase ejector improves energy efficiency by 12 to 60 %. Jin et al. [18] compared numerically the annual energy performance of two heat pump systems, "hybrid air/ground source and air source only" heat pump using R744 and R410A as refrigerants. Simulation results showed that the annual COP$_c$ and COP$_h$ for the hybrid R744 heat pump reach 3.55 and 3.22, respectively, and its cooling performance is better than the air source heat pump ASHP for the same refrigerant. While the annual system performance of the R410A ASHP system is better than the R744 hybrid system, the cooling performance of the R410A system seriously decreases when the ambient temperature is higher than 30 °C.

1.4. Building's energy modeling

On the other hand, building energy modeling that could accurately predict the thermal loads is crucial in optimizing the building performance and the adopted heating ventilation air conditioning HVAC system technology [19]. There are multiple modeling techniques, such as the black box models, i.e. data-driven or energy forecasting, that basically provide an efficient feedback platform to identify faults in energy consumption and energy efficiency opportunities and to improve decision-making for energy management in buildings [20]. White box modeling can be either self-developed codes or implementing any of the building dynamic energy simulation tools (BES) such as (EnergyPlus [21], TRNSYS [22], IDA ICE [23], and Modelica/Dymola [24]). These tools are increasingly used in research and consultancy-commercial levels [20]. It is important to emphasize that utilizing any of the tools above requires user expertise to assure the accuracy and quality of the results.

Moreover, the modeling and simulation process can be time-consuming in terms of computational cost and modeler effort [25]. Meanwhile, accessing the model source code is considered a positive side because it simply allows the modeler to comprehend more of the existing code if any, and tailor the equations to perfectly suit the specific case study [20]. This is where the Modelica language becomes one of the important engineering programing languages. It supports the acausal connection of components governed by mathematical equations to facilitate modeling from first principles and provides object-oriented constructs that enable the reuse of models and can be used conveniently for modeling complex systems [26]. All of this has led to the development of the **Spawn-of-Energy-Plus** [27], which is the next generation of the EnergyPlus BES tool. Spawn breaks EnergyPlus [21] into a set of component models with clearly defined input and output ports. It instantiates these components and their connections from the EnergyPlus input file, thereby not disrupting applications that use EnergyPlus, and then simulates them using a discrete event simulator [28].

To the authors' knowledge, the dynamic modeling of a high-fidelity small office reference building model [29] represented by Spawn connected to a complex air-cooled CO_2 chiller under different weather conditions in Chicago Oslo, and Athens was not investigated before. Moreover, the current study includes a comparative analysis of two scenarios for implementing the CO_2 chiller: with and without heat recovery. This comparison highlighted the induced differences in energy consumption and system performances. Finally, an evaluation review and steps of how to implement the newly released DOE component Spawn of EnergyPlus are discussed.

2. System general description

The study compares numerically; the performance of a CO_2 chiller with a nominal cooling capacity of 10 kW implemented to meet the thermal requirements of two thermal zones via direct exchange DX evaporator with and without heat recovery.

The piping and instruments diagram PID of the WHR and WOHR cases are shown respectively in Fig. 1.a and Fig. 1.c where the system components are denoted by Arabic numbers and thermodynamics cycle points are denoted by the Latin alphabet. Table 1 highlights the
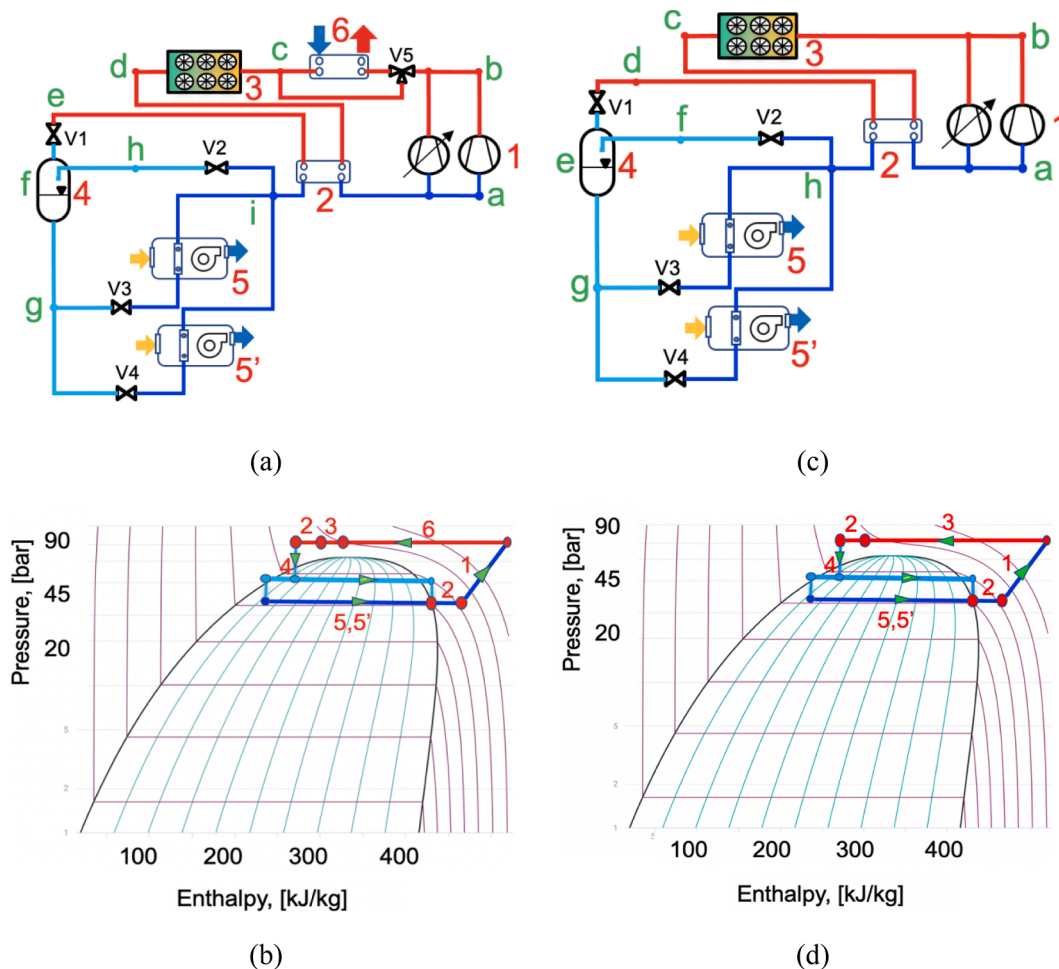

Fig. 1. CO_2 chiller system scenarios, a) WHR PID, b) WHR pH diagram, c) W/O HR PID, d) W/O HR pH diagram.

Table 1
CO_2 Thermodynamics cycles design data.

Case State point	WHR Pressure (bar)	Enthalpy (kJ. kg^{-1})	T (C)	WOHR Pressure (bar)	Enthalpy (kJ. kg^{-1})	T (C)
a	40	458	19	40	450	15
b	90	483	85	90	479	80
c	90	290	28	90	325	37
d	90	290	28	90	305	35
e	90	272	24	90	305	10
f	45	272	10	45	225	10
g	45	225	10	45	425	10
h	45	425	10	40	430	7
i	40	438	7			

thermodynamics cycle design data points for both cases.

The main components of the cooling system with heat recovery WHR as shown in Fig. 1.a include; two compressors(1), internal heat exchanger IHX(2), heat recovery heat exchanger HRHX(6), gas cooler GC(3), Liquid receiver(4), two fins and tube cross flow HX(5,5′) i.e. DX evaporators. Meanwhile, the case without heat recovery WOHR includes those above apart from the HRHX(6).

2.1. Thermodynamics of the with heat recovery "WHR" case

The hot gas is discharged from the compressor(s)(1) and flows into the HRHX(6) before entering the gas cooler GC(3), followed by the internal heat exchanger IHX(2) and the high-pressure valve [V1]. The refrigerant exit temperature from the GC(3) is a function of its size and ambient temperature. Depending on this exit temperature value, the control system decides the set-point for the high side pressure level, subcritical or *trans*-critical. In addition, the gas cooler variable frequency fan is controlled to maintain an approach temperature of 5 K. See section 4.2.a for more details.

The high-pressure gas expands through the high-pressure control valve [V1] to the separator setpoint pressure, and the resultant liquid/gas is separated in the separator(4). The gas expands through the flash gas bypass valve FGV [V2] to maintain the separator's pressure level by throttling a dedicated amount of vapor towards the compressor suction port. While the liquid leaves the separator(4) at the bottom towards the DX1 and DX2 evaporators.

The electronic feeding valves [V3] and [V4] were controlled to maintain slightly overfeed evaporators with a superheating SH setpoint value of 0.5 K.

Downstream of each DX evaporator (5,5′), the internal heat exchanger IHX(2) ensures a superheated vapor is fed to the compressor (s) (1), see more details in section 4.1. The thermodynamic CO_2 P-h cycle is illustrated in Fig. 1.b where the refrigerant leaves the HRHX[6] (thermodynamic process 6) followed by the GC(3) (thermodynamic process 3, identifying the high-pressure HP) and is subcooled through IHX(2) (thermodynamic process 2). Later it expands through the high-pressure control valve HPV (thermodynamic state 4). The mixed vapor/ liquid fluid is separated while the liquid is expanded into the evaporator's pressure level. The saturated vapor leaving the DX evaporator(s) (thermodynamic process 5,5′) is mixed with the expanded and superheated flash gas through [V2] before entering the IHX(2) (thermodynamic process 2). To complete the cycle, the hot vapor mixture is compressed through the compressors set to the HP design value (thermodynamics process1).

The heat flow recovered from HX(6) Q_{HRHX} is evaluated from Eqn.1

$$Q_{HR} = \dot{m}_{heaW}.c_w.(T_{heaWOutlet} - T_{heaWInlet})$$ (1)

Where, $\dot{m}_{heaW}$, is the heating water flow rate in (kg/s), c_w, is the water-specific heat capacity in (kJ.kg^{-1} K^{-1}), $T_{heaWOutlet}$ and $T_{heaWInlet}$, is the heating water leaving/entering the HX(6) in (K).

2.2. Thermodynamics of the without heat recovery "WOHR" case

The thermodynamic cycle description is similar to the latter case apart from utilizing only the gas cooler as a heat sink, Accordingly, the gas cooler's rejection heat flow (thermodynamic process 3) is expected to be larger than the WHR case. Fig. 1.d illustrates the system P-h cycle.

3. Numerical modeling

The models were developed using the Modelica language and Modelica standard libraryV3.2.3 [30]. Different components were either instantiated from the TIL 3.9.1 commercial Modelica library[31], the open-source Modelica Buildings library MBL V9.0.0 [32], or developed from scratch. Modelica environment, i.e. Dymola2022 [24], is used to run the different models with a Cvode solver and 1e⁻⁴ tolerance. The effects of oil and oil management system are neglected.

3.1. The Air-cooled chiller consists of:

Referring to the components numbering in Fig. 1.a and Fig. 1.c. The implemented modulating valves [V1] to [V4] use the Bernoulli equation Eqn.2, which is used to calculate the mass flow rate in dependency on the pressure drop between the valve's inlet and outlet ports

$$\dot{m}_{ref} = A_{eff}.\sqrt{\Delta p.2\rho_{in}}.$$ (2)

Where, $\dot{m}_{ref}$ is the refrigerant mass flow rate in (kg s^{-1}), Δp is the pressure gradient across the valve in (pa), ρ_{in} is the inlet flow density in (kg m^{-3}). A_{eff} is the valve cross-sectional area which the flow passes through changes in (m^2) defined in Eqn.3

$$A_{eff} = k_v\sqrt{\frac{\rho_{in}}{2p_{1bar}}}$$ (3)

Where, k_v is the volume flow rate for a pressure loss of 1 bar (m^3h^{-1}), p_{1bar} is the pressure loss of 1 bar, ρ_{in} is the inlet flow density in (kg m^{-3}).

The gas cooler GC(3) is modeled as a fin and tube cross-flow heat exchanger type with a heat transfer area equal to 12.5 m^2. The heat transfer coefficient on the refrigerant side was estimated to be 3000 W. $m^{-2}K^{-1}$ [33]. The HRHX(6) is modeled as a plate cross-flow heat exchanger type with a heat transfer area equal to 15.5 m^2. Two compressors(1), one is a variable frequency compressor (varFC), where its rotational speed RPM is modulated to maintain the suction pressure at the setpoint value. While the other is the constant frequency compressor (conFC) On/Off control type. The compressor is modeled using performance coefficient correlations which are a function of some suction and delivery variables such as pressure and temperature. These coefficients include the mass flow rate, and the compressor consumed electrical power are derived from performance schedules published by the manufacturer [34]. The number of active compressors is determined by a stage up/down controller based on the maximum value of measured air temperature (plus the hysteresis) between both thermal zones; more details in section 4.1. A liquid receiver(4) of 30 L is implemented in the system, where its pressure level is maintained at (45 bar) by modulating the FGV [V2] opening ratio, i.e. the effective area to expand a specific amount of vapor from the receiver to the compressor's suction manifold.

The DX evaporator [5,5′] is modeled as a fin and tube heat exchanger with a heat transfer area of 5.5 m^2. Handling the moist air is essential with SPAWN thermal zones when there is a source of latent load. Otherwise, the humidity content builds up until the relative humidity reaches 100 %, and the model stops and fails. A moist submodule is included in the DX evaporator, where the condensation and evaporation of water are considered, using a dynamic mass and energy balance of the water film. The heat transfer coefficient was evaluated as 2500 W/m^2K [33]. The evaporator's variable frequency-driven fan is controlled to maintain the room air temperature at a set point equal to 24C [35]. The fresh air flow rate is evaluated as per ASHRAE Standards

recommendations [36] of 9.4(l/s)/person, and for the model simplicity, it is considered non-treated, i.e., the fresh air flow from the ambient was connected directly to the mixing air volume of the Spawn thermal zone. Each DX evaporator is equipped with a modulating effective flow area feed valve [V3, V4], which it is controlled to maintain the design superheating SH value.

3.2. Thermal zone modeled by "Spawn"

EnergyPlus is a credible and well-known software implemented to simulate the whole building energy and indoor comfort performance and has been used worldwide for 25 years [20]. Meanwhile, the software has some shortcomings such as difficulty in integrating building energy modeling BEM with control workflows that mimic the actual control systems. This is where the importance of **Spawn-of-Energy-Plus** as a high-fidelity building simulation tool appears, as the user can link through it, EnergyPlus to the advanced HVAC and control systems developed on Modelica. Spawn is a Modelica component [27], instantiated from the MBL [32], and is used to perform a whole building energy simulation. It uses the functional mockup interface FMI [37] to link the building envelope and daylight modules of EnergyPlus [21] with the HVAC and control systems on Modelica.

Spawn's users can analyze and demonstrate results retrieved from both the Modelica side and the long list of outputs available on the EnergyPlus side [38], using a component called "output variables" instantiated from the MBL. Other helpful features such as the modeling of opaque surfaces, writing to EnergyPlus actuator(s), or working schedules during the simulation and setting individual surface temperatures in EnergyPlus are also included in Spawn. Two essential steps the user must follow to implement Spawn successfully; first, define the thermal zone characteristics on the input data file IDF and load it with the weather file to the "building" instance from the MBL. The second step is to develop the HVAC control system in Modelica, connect it to the Spawn component, and run it on the Modelica environment.

3.2.1. Dynamic energy balance

The basic idea behind SPAWN lies in exchanging Modelica variables of the room air heat, mass flow rate, and pressure balance with the EnergyPlus thermal zone models that compute the radiative and convective heat gains from building's fabrics, internal loads, and solar gains. The energy balance of the thermal zone is evaluated from Eqn.4

$$U = \int_{t_i}^{t} \left(Q_{total} + EntFlowSpawn \right) \tag{4}$$

Where, U is the system's internal energy due to the zone air temperature changing from one timestep to the next in (J), Q_{total} is the summation of exchanged sensible and latent heat flow between EnergyPlus and Modelica sides in (W), EntFlowSpawn (W) is the sum of the enthalpy flows connected through Spawn fluid ports in (W) and is evaluated from Eqn.5.

$$EntFlowSpawn = \sum \dot{m}_{air} . h_{flow} \tag{5}$$

Where, $\dot{m}_{air}$ is the sum of the airflow rate of all fluid ports connected to the Spawn component in (kg/s), i.e. entering (positive sign) and leaving (negative sign), i.e. according to the Modelica conventions [26], h_{flow} is the enthalpy of the airflow in (J kg^{-1}). The building utilized in the current study is a DOE reference small office building [39] from which we modeled two thermal zones. Table 2 summarizes thermal zone design specifications, and Fig. 2 illustrates the occupancy availability in percentage through the day hours.

3.3. Key performance indicators KPI'S

The primary performance indicator implemented in this study is the coefficient of performance COP and is evaluated for the WHR by Eqn.6

Table 2
Thermal zones input data.

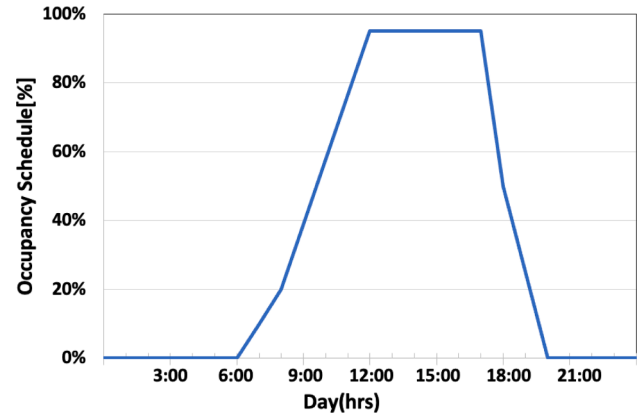| Thermal zone	Area (m²)	Internal gains		
		Area per Person (m² /person)	Light (W. m^{-2})	Electric equipment (W.m^{-2})
Zone1	149.6	18.58	10.76	10.76
Zone2	113.4	18.58	10.76	10.76

Fig. 2. Daily Occupancy schedule %.

and WOHR by Eqn.7.

$$COP_{WHR} = \frac{Q_{HR} + Q_{Eva}}{P_{Com} + P_{gcFan}} \tag{6}$$

$$COP_{WOHR} = \frac{Q_{Eva}}{P_{Com} + P_{gcFan}} \tag{7}$$

Where, Q_{HR} is heat recovery heat flow in (W), Q_{Eva} is the evaporator (s) heat flow in (W), $P_{Com} and P_{gcFan}$ are the compressor(s) and gas cooler fan electrical power in (W) respectively.

4. Control system

The control system employed at the two-phase medium models in Modelica is a role player because it tracks and maintains the design setpoints and assures a smooth-running simulation with an adequate CPU time.

4.1. Control system description

The control algorithm consists of hierarchical layers, as shown in Fig. 3, where the first layer includes the supervisory controller, which evaluates:

i) number of the active compressor where a state machine is implemented to stage up and down the number based on the measured values of the room air temperature plus the hysteresis, i.e. to avoid short cycling. It is worth mentioning that the compressor controller is equipped with a safety measure that allows to control the feeding valves [V3, V4] of the evaporators in case the SH was lower than 5 K.

ii) the reset value of the high-pressure level setpoint based on the temperature of the refrigerant leaving the gas cooler.

It is worth mentioning that the high-pressure level has an important influence on the performance of the CO_2 system. However, Yang et al. [40] have shown that the standard deviation SD of implementing linear correlation proposed by Liao, Zhao and Jakobsen [41] is ≤ 1 %. Hence, the continuous reset of the high-pressure setpoint is evaluated according
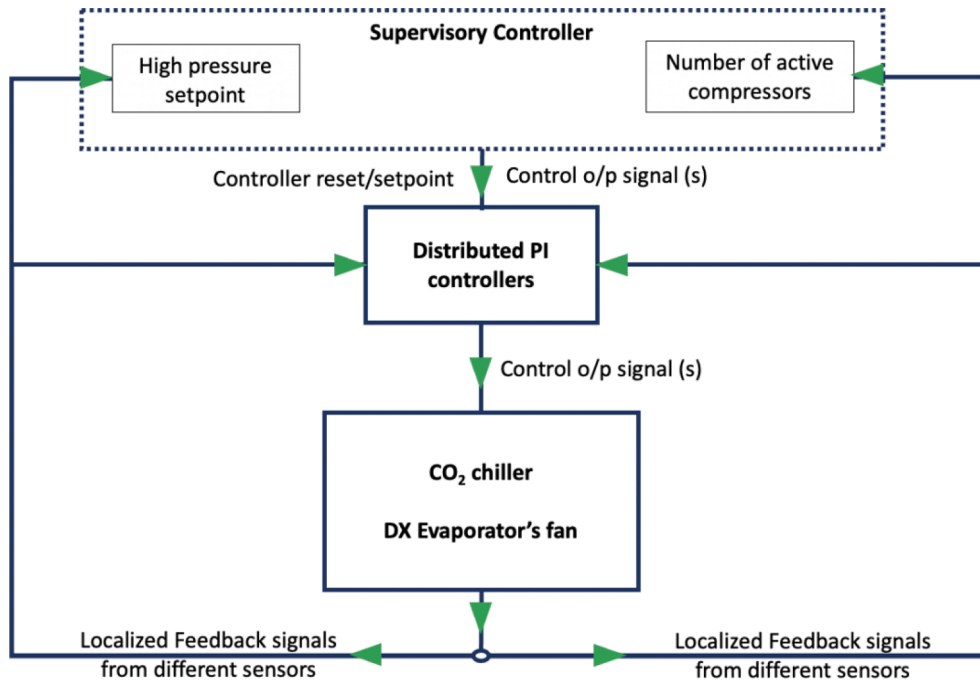
Fig. 3. Hierarchical control description.

to the linear equation Eqn.8;

$$HP_{set} = 2.3T_{gcout} + 9.5[bar] \tag{8}$$

The second layer includes the different distributed proportional-integral PI controllers implemented to track:

- The CO_2 chiller sub-components as the variable frequency compressor, the gas cooler fan, the modulating feed valves of the two evaporators, the high-pressure level valve, and the flash gas valve.
- DX evaporator fan speed.

The localized feedback signals are generated from various sensors that measure temperature and pressure values.

It is worth mentioning that for the WHR case, a continuous heat flow is assumed with a water mass flow rate controller that ranges between 0.02 and 0.06 kg s^{-1} to maintain the $T_{heaWOutlet}$ at 70 °C, while $T_{heaWInlet}$ is assumed to be a boundary condition equals to 20 °C.

4.2. Maximize system efficiency

Controls are an increasingly important part of building energy-efficiency and building-to-grid integration, simply by changing the control sequence, building HVAC energy use can be reduced by 30 % [42]. Accordingly, two control items have been considered in this study to maximize the system efficiency:

a- Gas cooler fan RPM.

As the gas cooler air mass flow rate is a controlled variable, the frequency of the gas cooler fan is controlled to maintain the approach temperature T_{AppAbs} Eqn.9 at the setpoint of 5 K.

$$T_{AppAbs} = T_{gcout} - T_{ambDB} \tag{9}$$

Where, T_{gcout} and T_{ambDB} are the refrigerant leaving the gas cooler temperature, and the ambient dry bulb temperature in (K) respectively, T_{AppAbs} is the absolute approach temperature in (K).

b- Reset the suction pressure setpoint.

As mentioned earlier, the varFC compressor is modulated to maintain the suction pressure at the design value. However, this approach might lead to higher energy consumption during the non-peak hours.

Hence, Eqn.10 was derived with a pressure upper limit value of 46 bar and a lower limit value of 42 bar to continuously reset the suction pressure setpoint as a function of the measured thermal zone air temperature.

$$p_{SucReset} = -2T_{Air} + 92 \tag{10}$$

Where, T_{Air} is the measured air temperature in (C), $p_{SucReset}$ is the setpoint suction pressure in (bar).

5. Results

The simulation time is adjusted to start on the 29th of July until the 2nd of August. However, the more in-depth analysis was highlighted on the 2nd of August because it recorded the highest ambient temperature of 37 °C in Athens.

5.1. WHR scenario

As explained previously, the high-pressure level reset is a function of the refrigerant temperature leaving the GC. Hence the HP setpoint value is directly correlated to the ambient dry bulb temperature, as shown in Fig. 4 and Fig. 5, respectively. As the ambient temperature rises, which indicates the increment in the cooling demands, the high-pressure
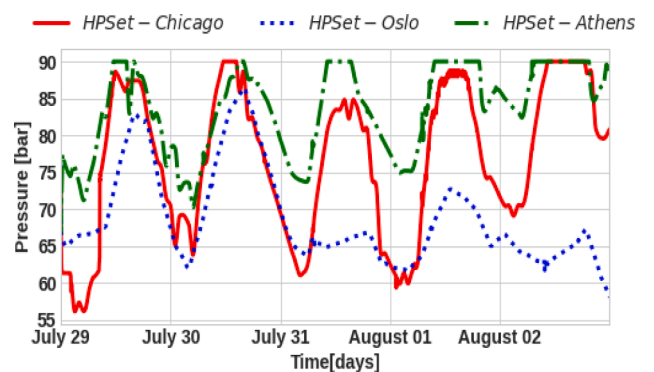

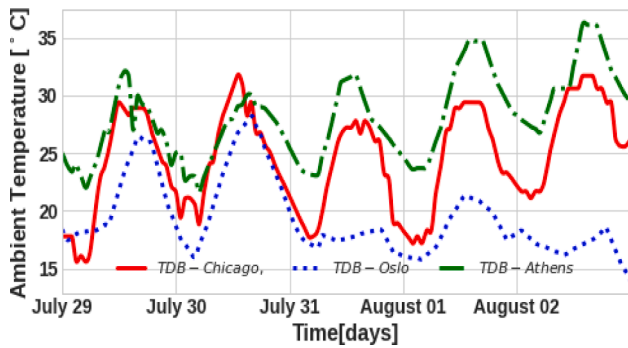**Fig. 4.** WHR case Reset of the high-pressure level.

Fig. 5. Ambient dry bulb temperature.

setpoint trajectory in Athens increases gradually until it reaches its maximum value of 90 bar. Chicago and Oslo cities follow the same pattern every day; however, in the case of Oslo, it doesn't reach the maximum value of 90 bar due to the lower ambient temperature and cooling demands.

- Thermal Zones air temperature

On the 2nd of August, as shown in Fig. 6.a and Fig. 6.b, the chiller system in Chicago is switched ON by 7:00 am when the internal gains schedule of people, equipment, and lights is utilized. The air temperature profiles for thermal zones one and two lies within the thresholds of activating only the varFC compressor. On the other hand, in Oslo, switching the chiller system ON is delayed for about 30 min compared to the latter city as the increment of the air temperature of zone one and two were below the threshold of activating the system at 7:00 am. Meanwhile, the chiller system in Athens's city starts operating by 7 am when the air temperature of thermal Zone1 reaches 24.5C, i.e. air design temperature value plus the hysteresis as shown in Fig. 6.a and Fig. 7.b.

- System's compressors status

In Chicago, the varFC RPM increases gradually till it reaches its maximum value of 70 Hz by 10:30 am coinciding with the increment in the internal gains profile as shown in Fig. 7.a and Fig. 8.a. The compressor RPM declines gradually by 5 pm through 7 pm, i.e. the end of the working hours. For Oslo, the varFC compressor's RPM runs on an average value of 38 Hz to maintain the design air temperature of 24℃. By 14:00, RPM increases gradually, coinciding with the increment of the internal gains, and declines back again to its minimum value of 30 Hz. The chiller unit is switched OFF by 7 pm, as shown in Fig. 7.a and Fig. 8.a.

As a result of the relatively higher ambient temperature of Athens compared to the latter cases, the varFC compressor's RPM is increased till it reaches 70 Hz for a couple of hours before zone 2's indoor air temperature reaches 25C̄, i.e. the threshold of switching ON the second constant RPM compressor conFC as illustrated in Fig. 6b and 7b. Switching ON the second compressor causes the pressure at the compressor's suction manifold to drop, which motivates the varFC's controller to decrease the RPM to its minimum value of 30 Hz to compensate for such a pressure drop. The varFC's frequency increases till it reaches the maximum value of 70 Hz. The conFC is switched OFF by 16:00 after passing the peak load period while the conFC is switched OFF by 7:00 pm. As expected, during the working hours, the compressors' electrical energy consumption in Athens was the highest at 29 kWh/day. Chicago city came second with 25 kWh/day. At the same time, Oslo city is the lowest electrical energy consumption of 5.5 kWh/day. The chiller unit performance parameters for the three cities are summarized in Table3.

- Thermal zones cooling demands

Although the second of August records the maximum ambient temperature of 37℃ in Athens, the cooling energy of Chicago city was higher with about 4 kWh/day. The reason behind this difference is the ambient humidity ratio, as shown in Fig. 9 Chicago has the highest trajectory. Accordingly, the latent loads induced by the ventilation loads were higher in Chicago by about 15 %. The sensible heat ratio SHR profiles of Zone1 and Zone2 in Chicago and Athens are illustrated in Fig. 10.a and 10.b resepctively.

5.2. Comparison between the WHR and WOHR scenarios

In this section, we analyze and compare the influence of implementing heat recovery to null on some of the system variables such as high-pressure side setpoint, the system COP, and the approach temperature.

a- High-pressure side setpoint.

The results have demonstrated a few differences between the WHR and the WOHR scenarios. As shown in Fig. 4 and Fig. 11, the reset of the high-pressure setpoint for the WOHR is slightly above the former case in Oslo. As for the other two cities and for the WOHR, the maximum value of 90 bar is reached earlier through the day hours compared to the WHR case.

b- Energy performance.

The main system's improvement lies within the COP value, since the heat recovery HR is i) generating a by-product, i.e. bonus heating energy, and ii) reducing the gas cooler fan's electrical energy consumption. In Oslo and for the "WHR case," the gas cooler is almost bypassed, while
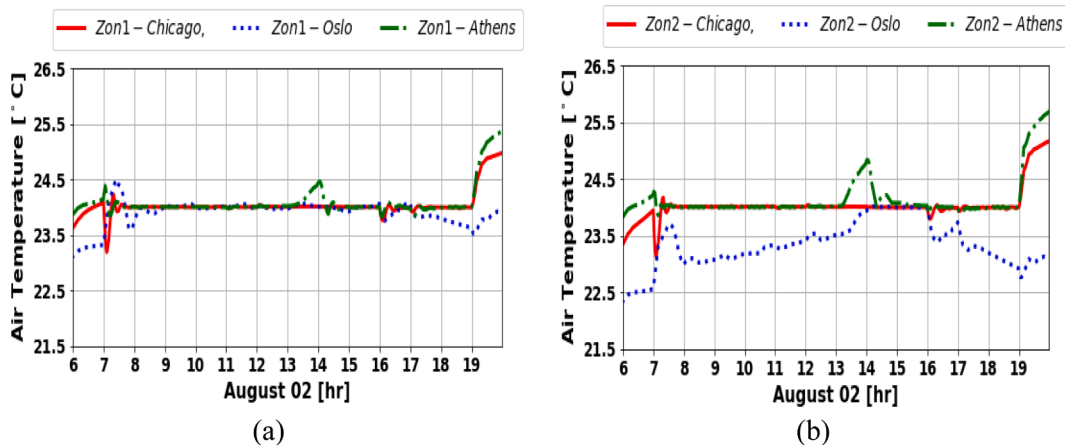

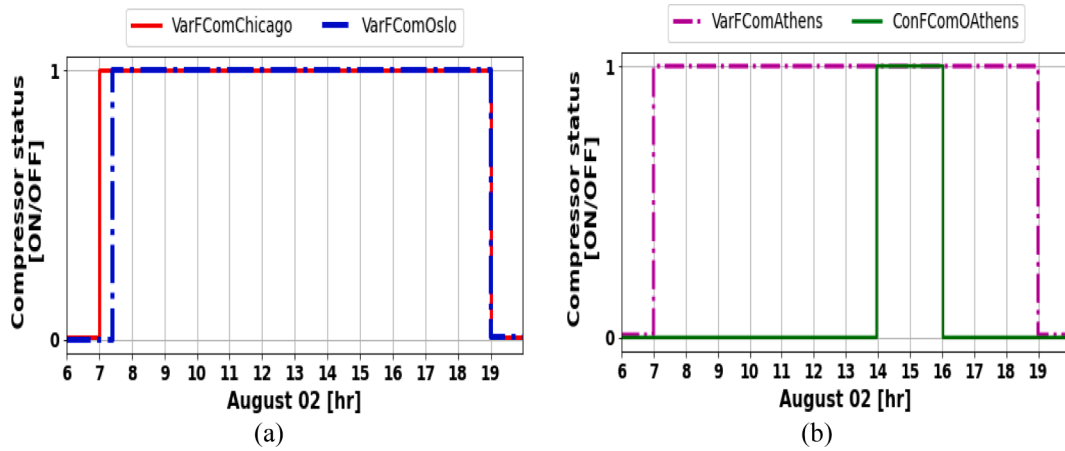**Fig. 6.** Air Temperature, a) thermal zone 1, b) thermal zone 2.

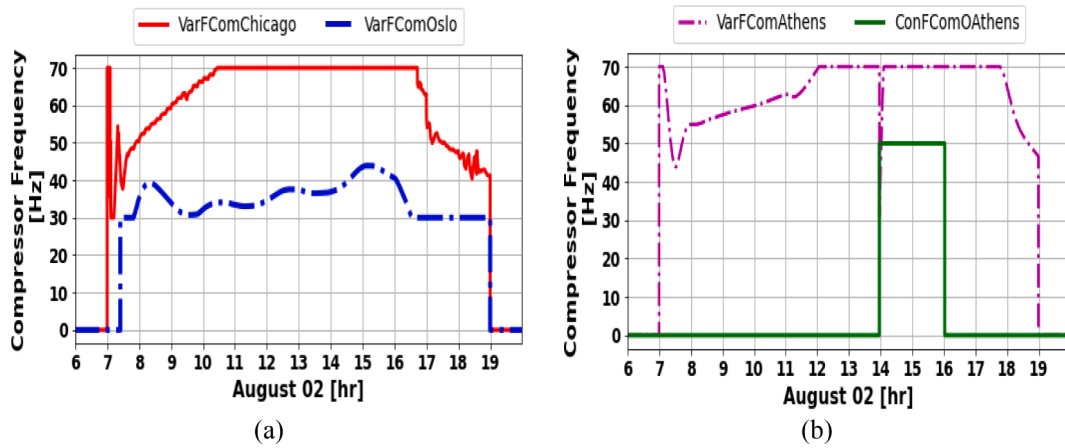**Fig. 7.** Compressor(s) status at different cities a) Chicago and Oslo cities, b)Athens city.

Fig. 8. Compressor(s) RPM at different cities a) Chicago and Oslo cities, b) Athens city.

Table 3
WHR CO$_2$ Chiller system performance.

City	Cooling energy (kWh/day)	Heating energy (kWh/day)
Chicago	88.0	54
Oslo	40.0	–
Athens	84.0	68
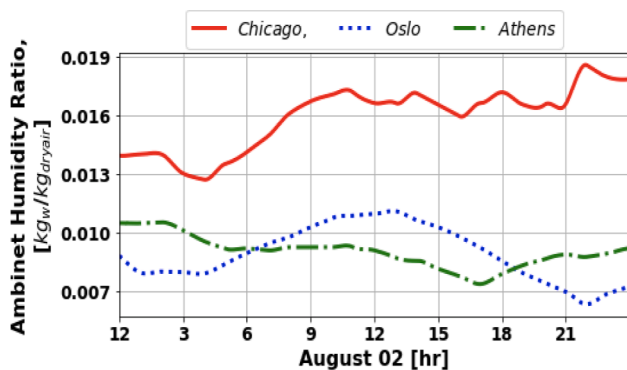
Fig. 9. Ambient humidity content of the three cities.

in Chicago, the gas cooler fan's electrical energy consumption reached 1kWh per day, and in Athens, it reached 2 kWh/day. While for the "WOHR case," Athens's city recorded the maximum gas cooler's fan electrical energy consumption of 9 kWh/day. Chicago and Oslo cities recorded 5 and 2 kWh/day, respectively. Table 4 demonstrates the average COP for the two scenarios in the three cities.

c- Gas cooler approach temperature.

To evaluate the influence of the heat recovery utilization on the approach temperature, especially in a relatively hot climate such as the Athens city case, the gas cooler fan PI controller was replaced with a constant input air flow signal equal to 3 kg s^{-1}, i.e. the maximum fan flow rate. The results demonstrated that the average approach temperature is equal to 1.5 K for the WHR case. While it is almost doubled for the WOHR case to 3.2 K, as shown in Fig. 12.

6. Discussion

6.1. Short cycling and compressors capacity

The short cycle is a term that describes incorrect sizing and pressure settings for a set of varFC and conFC compressors, which results in unstable system operation. The main idea of utilizing a group of compressors is to guarantee smooth operation during part load by correctly designing the size of the varFC compressor. As shown in Fig. 13, the displacement volume flow rate of the VFC running at the maximum frequency of 70 Hz(c) has to be larger than the displacement volume flow rate of the varFC running at the minimum frequency of 30 Hz(a)
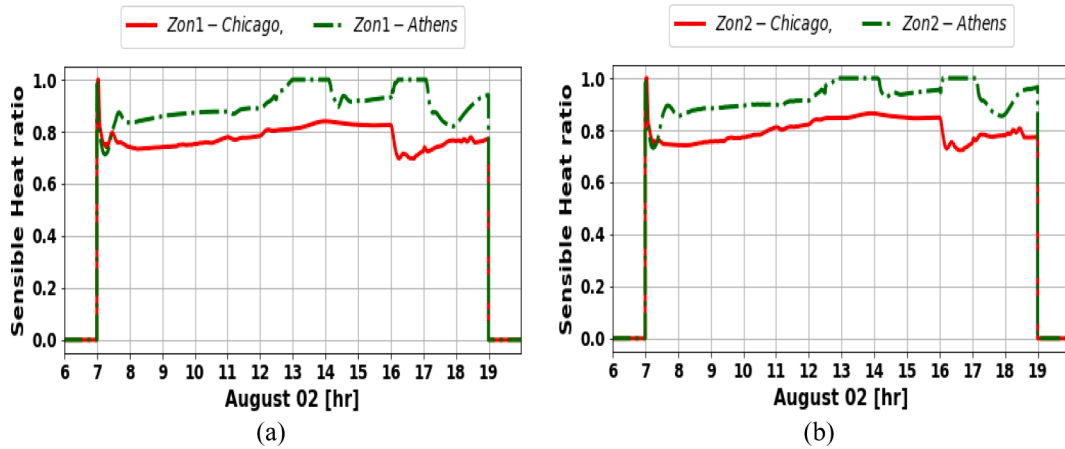
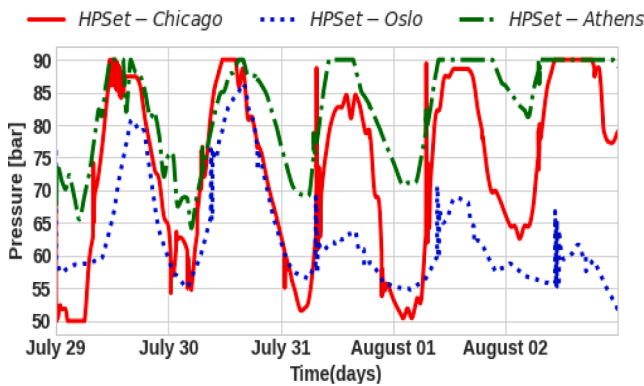Fig. 10. Sensible heat ratio, a) Zone1, b) Zone2.

Fig. 11. W/O HR case, Reset of the high-pressure level.

Table 4

COP of the CO_2 Chiller unit.

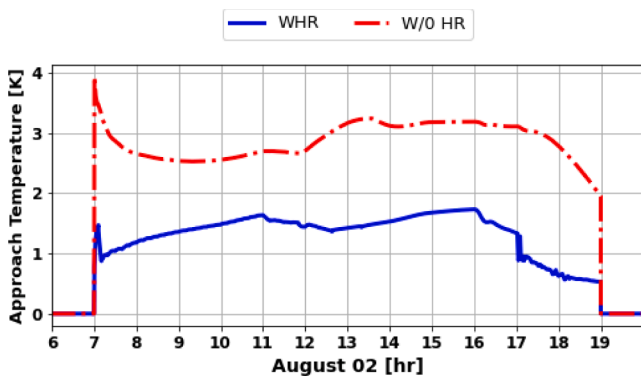| Scenario/City	Chicago	Oslo	Athens
COP_{WHR}	5.4	7.2	4.9
$COP_{W/O\ HR}$	2.9	5.3	2.2

Fig. 12. Gas cooler approach temperature in Athens city.

plus the displacement volume of the conFC running at a nominal frequency of 50 Hz (b). Hence, if the system load increases after the second conFC compressor is activated, the varFC would have more than 70 % of its maximum capacity to handle this load. The same capacity design rule applies for three compressor sets, one is varFC, and the other two are
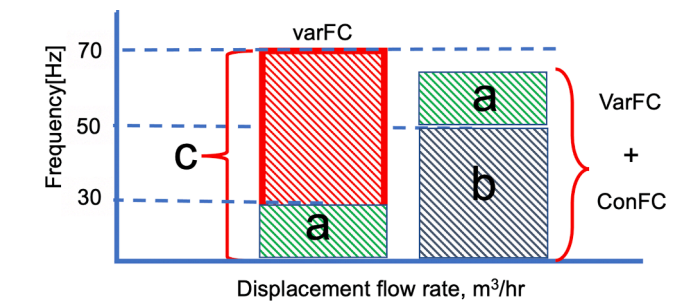

Fig. 13. Compressor(s) sizing.

Table 5

Compressor(s) capacities in (m^3/hr).

City	varFC ($m^3.hr^{-1}$)		conFC ($m^3.hr^{-1}$)
	(a) 30 Hz	**(c)** 70 Hz	**(b)** 50 Hz
Athens	1.1	2.6	1.0
Chicago	1.1	2.6	1.0
Oslo	0.7	1.8	1.0

conFC. Table5 demonstrates the sizing of different compressors associated with the three cities to avoid i) control gap, and ii) oversizing of the compressor(s) system.

6.2. Spawn outputs and tool review

This section discusses some of the building's thermal characteristics, which the user can retrieve from the Spawn component. In addition to an evaluation review of Spawn use in this study.

6.2.1. Spawn outputs
a- Relative Humidity analysis.

Since the relative humidity RH is not controlled, the daily profiles for the three cities under investigation, as shown in Fig. 14.a and 14.b, are floating. In Oslo city and until the chiller system is activated, the RH value inside the two thermal zones increases until it reaches 60.5 % due to the people's latent gains, i.e., humidification without cooling. The RH profile starts to decline through the day hours. In Chicago and Athens, the RH profiles range between 50 % ±8 and increase gradually with the occupancy rate. By the end of the working hours and the decrement in the humidity content induced by people's latent load, RH profiles start to decline. This behavior is due to the larger cooling and dehumidification demands compared to the Oslo case.
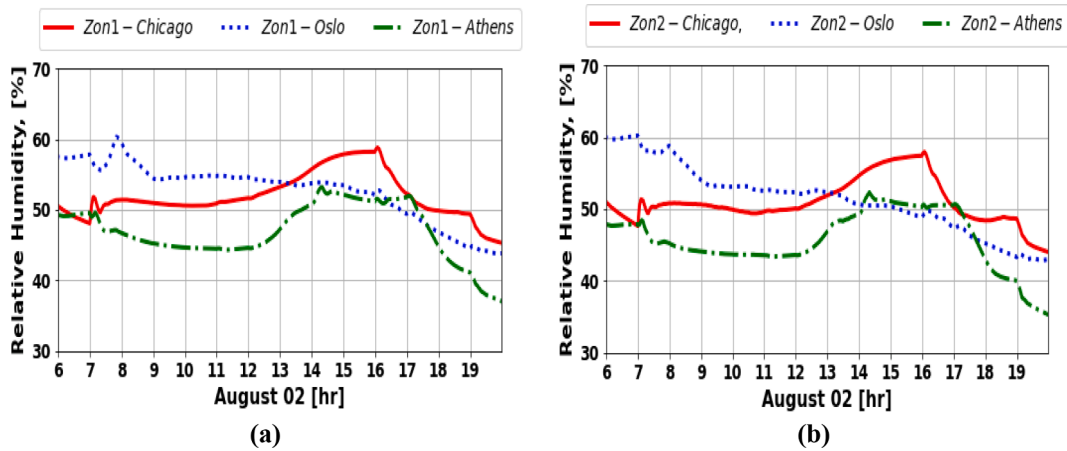
b- Dynamic thermal balance.

Fig. 14. Thermal zones Relative Humidity RH, a) Zone 1, b) Zone2.

One of the benefits of using Spawn is that the user can analyze in detail the dynamic performance of the thermal zone by retrieving some of Spawn's output variables such as Q_{total} and EntFlowSpawn Eqns [3] and [4]. As shown in Fig. 15.a,15.b and 15.c, the enthalpy flow for Zone1 matches the evaporator's cooling capacity for Chicago, Olso, and Athens, respectively.

On the other hand, a difference between the Q_{Tot} and EntFlowSpawn profiles was noticed in Chicago and Athens. This difference is due to the ventilation latent loads induced from mixing the nontreated fresh air directly into the thermal zone..

6.2.2. Review of Spawn as a modelling tool

- Although Spawn is considered an important tool to simulate the thermal performance of buildings, detailed documentation that explains different aspects of the Modelica component is still required. For example, the developers decided to connect the radiative heat gain variable of QGaiRad_flow as an input signal to the FMU block and not to the Modelica air volume directly, as shown in Fig. 16, i.e., the FMU block exchanges data between Modelica and EnergyPlus by calling the C + functions to initialize EnergyPlus [43]. This decision apparently was made since the Modelica mixing air volume
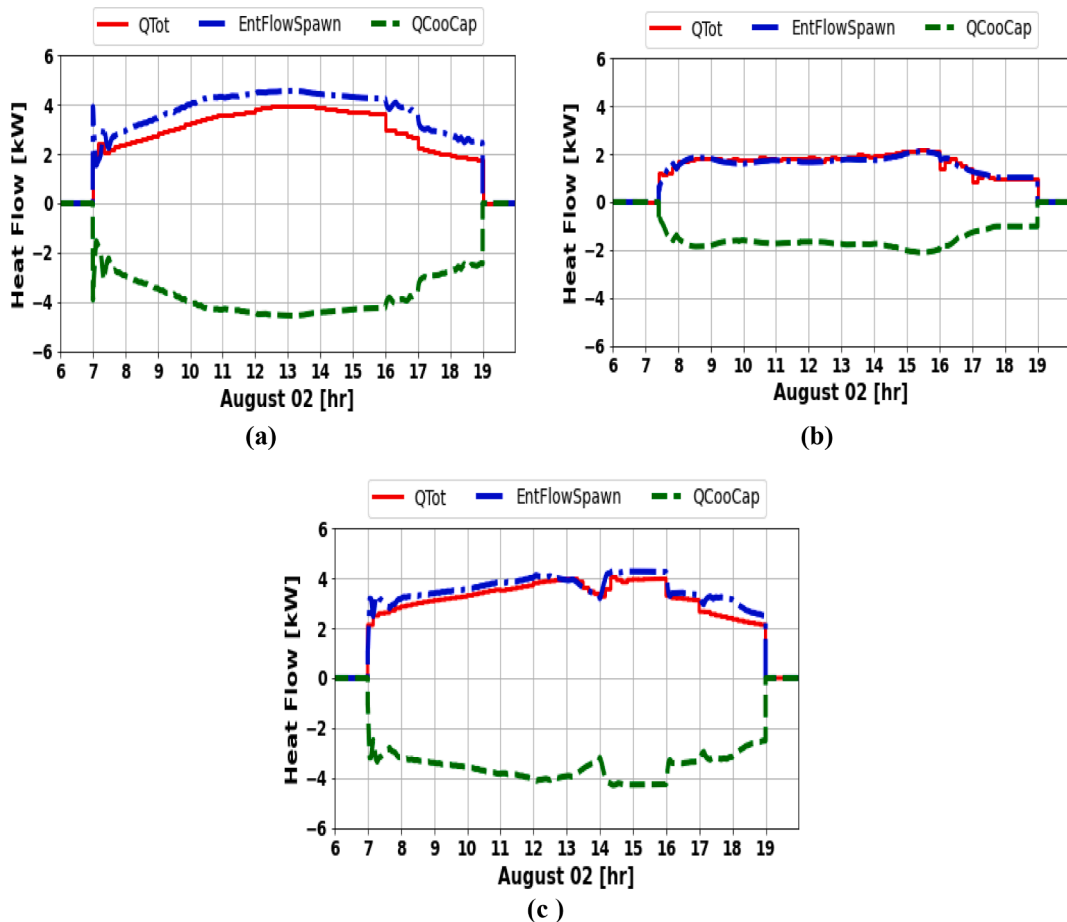

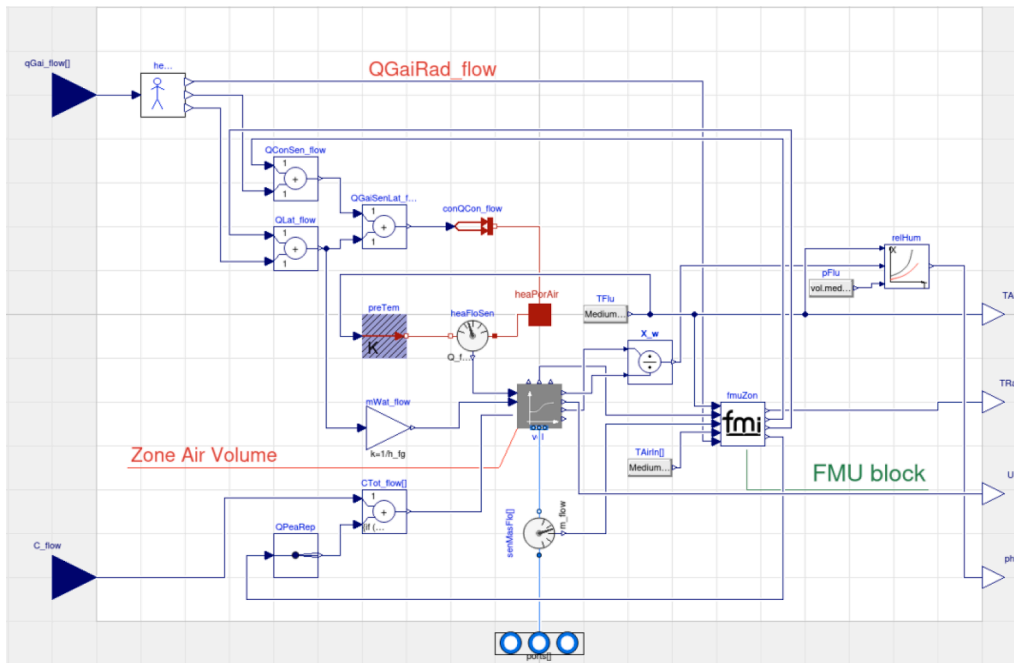**Fig. 15.** Energy balance of thermal Zone1, a) Chicago, b) Oslo, c)Athens.

Fig. 16. SPAWN Modelica component layout.

component doesn't include definitive surfaces. While each thermal zone on EnergyPlus is represented by a group of surfaces that shares in the overall radiation heat exchange balance. This un-clarified point might create confusion, especially for new users.

- Another issue we noticed while using Spawn is that U, i.e., the air internal energy value, is not connected to the EnergyPlus equivalent variable named "Zone Air Heat Balance Air Energy Storage Rate," as shown in Fig. 17 in Zone 1. It might be that the developers decided to ignore this output on the EnergyPlus side since the energy and mass balance of the thermal zone is executed on the Modelica side. However, it would be clearer to either synchronize the two variables or remove this EnergyPlus output variable from the Spawn output list [38].
- Computing time and technical specifications are important KPI's for any simulation tool. The current investigation was executed on virtual machine of Linux OS with RAM of 9 GB and a processor of 2.6 GHz core Intel Core I7. The computing time is 40sec for one day. Taking into consideration that computing time in Modelica depends on how the solution evolves by the solver through the continuous integration.
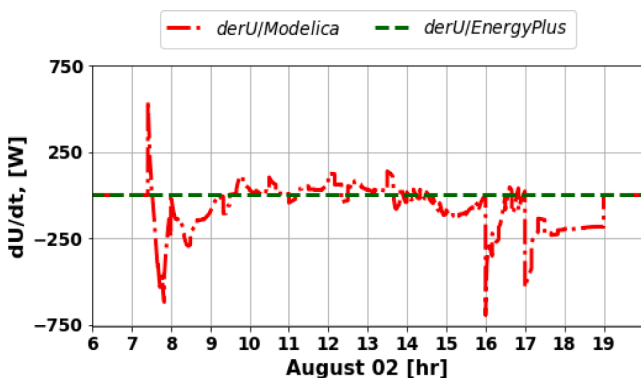
6.3. Heat recovery and smart control

In the present study and for the sake of simplicity, the heat recovery system is assumed to be working continuously. However, in real-life applications, a thermal energy storage system is required to decouple between the heat availability and the heat demand.

In addition to some control features to improve the system efficiency in hot and cold climate cities such as Athens and Oslo. These features include the synchronization between the high ambient temperature daytime period and activating the charging of the available thermal storage system. Another feature is resetting the high-pressure side to a value between 90 and 120 bar during heating demands and switching the reset step to Eqn.[7] during cooling-only demands. However, the utilization of such features is conditioned by having buildings with simultaneous heating and/or cooling demands, such as hotels.

7. Conclusions

Implementing clean refrigerants such as CO_2 is a promising solution to deaccelerate global warming. A CO_2 chiller unit integrated with heat recovery is an energy-efficient and environmentally friendly option for diverse building applications that require simultaneous heating and cooling demands. In this work, a detailed dynamic simulation model of a CO_2 chiller connected to a small office building represented via Spawn-of-Energy-Plus was developed. The results have shown improvements in the system COP, reaching 5 in relatively hot and moderate climates, as in Athens and Chicago, and 7 in a cold climate as in Oslo.

Higher values of outdoor humidity content affect the thermal zone sensible heat ratio and, accordingly, the indoor comfort as occurred in Chicago compared to Athens, especially when the ventilation is non-pretreated.

On the other hand, modeling in general, and Modelica programming language particularly, are becoming more popular as a credible research tool to investigate innovative and detailed solutions. Meanwhile, implementing Spawn-of-Energy-Plus as the latest DOE software release is a very good step towards a more detailed representation of building modeling. The current study has filled a gap that the building modeling research community is currently facing of not having case studies that connect Spawn to a detailed thermal system combined with a close-to-

Fig. 17. Derivative of the air energy storage rate.

reality control algorithm.

Future investigations include developing Spawn models integrated with advanced control algorithms and combined with thermal energy storage systems for different building applications such as supermarkets, hotels [44], and fishing vessels. These models will be validated against experimental data from the demonstration sites of INDEE + project [45].

Declaration of Competing Interest

The authors declare that they have no known competing financial interests or personal relationships that could have appeared to influence the work reported in this paper.

Data availability

The authors do not have permission to share data.

Acknowledgments

References

[1] European Commission in focus news: https://ec.europa.eu/info/news/focus-energy-efficiency-buildings-2020-lut-17_en, (Last access: 18-06-2022).

[2] R. Ciconkov, Refrigerants: There is still no vision for sustainable solutions, International Journal of Refrigeration 86 (2018) 441–448.

[3] G. Lorentzen, Revival of carbon dioxide as a refrigerant, International journal of refrigeration 5 (1994) 292–301, https://doi.org/10.1016/0140-7007(94)90059-0.

[4] Hafner A., Pardiñas, Á.Á., 2019. CO_2 Refrigeration Technology: possible innovations. Proceedings of the IIR Conference: Ammonia and CO_2 refrigeration technologies, Ohrid, Macedonia, 173-180.

[5] Sawalha, S. (2008). Carbon Dioxide in Supermarket Refrigeration (Ph.D. dissertation, KTH). Retrieved from http://urn.kb.se/resolve?urn=urn:nbn:se:kth:diva-4753, (Last access: 18-06-2022).

[6] Kauffeld, M. (Hrsg.); Siegismund, V. (Hrsg.): Natürliche Kältemittel: Anwendungen und Praxiserfahrungen. Berlin and Offenbach and Karlsruhe: VDE Verlag GmbH and cci Dialog GmbH, 2019 (cci Buch). ± ISBN 9783800739363.

[7] J. Luo, K. Yang, Z. Zhao, G. Chena, Q. Wang, Experimental investigations on the performance of a single-stage compound air-source heat pump using CO_2/R600a in cold regions, Applied Thermal Engineering (2022) 11805, https://doi.org/10.1016/j.applthermaleng.2022.118050.

[8] Q. Cui, C. Wang, E. Gao, X. Zhang, Pinch point characteristics and performance evaluation of CO_2 heat pump water heater under variable working conditions, Applied Thermal Engineering 207 (2022), 118208, https://doi.org/10.1016/j.applthermaleng.2022.118208.

[9] Á.Á. Pardiñas, A. Hafner, K. Banasiak, Novel integrated CO_2 vapor compression racks for supermarkets. Thermodynamic analysis of possible system configurations and influence of operational conditions, Applied Thermal Engineering 131 (2018) 1008–1025, https://doi.org/10.1016/j.applthermaleng.2017.12.015.

[10] http://www.enob.info/(Last access- 18-06-2022)10.

[11] Réhault, N. and Kalz, D., 2012. Ongoing Commissioning of a high-efficiency supermarket with a ground-coupled carbon dioxide refrigeration plant. https://hdl.handle.net/1969.1/148917.

[12] Minetto, S., Condotta, M., Rossetti, A., Girotto, S. and Del Col, D., 2016. Ejector CO_2 heat pump for space heating and cooling. In12th IIR Gustav Lorentzen Conference on Natural Refrigerants, Edinburgh, Scotland. https://doi.org/10.18462/iir.gl.2016.1073.

[13] G. Maouris, E.J.S. Escriva, S. Acha, N. Shah, C.N. Markides, CO_2 refrigeration system heat recovery and thermal storage modeling for space heating provision in supermarkets: An integrated approach, Applied Energy 264 (2020), 114722, https://doi.org/10.1016/j.apenergy.2020.114722.

[14] Á.Á. Pardiñas, M. Jokiel, C. Schlemminger, H. Selvnes, A. Hafner, Modeling of a CO_2-Based Integrated Refrigeration System for Supermarkets, Energies 14 (21) (2021) 6926, https://doi.org/10.3390/en14216926.

[15] Pardiñas, Á.Á., Hafner, A., Banasiak, K., Kvalsvik, K.H. and Larsen, L., 2018. Strategy for the control of two groups of ejectors operating in parallel in integrated R744 refrigeration systems. In Proceedings of the 13th IIR Gustav Lorentzen Conference, Valencia, 2018. IIR.

[16] S. Sawalha, Investigation of heat recovery in CO_2 trans-critical solution for supermarket refrigeration, International journal of refrigeration 36 (1) (2013) 145–156, https://doi.org/10.1016/j.ijrefrig.2012.10.020.

[17] Z. Jin, A. Hafner, T.M. Eikevik, P. Nekså, Preliminary study on CO_2 transcritical ejector enhanced compressor refrigeration system for independent space cooling and dehumidification, International Journal of Refrigeration 100 (2019) 13–20, https://doi.org/10.1016/j.ijrefrig.2019.01.027.

[18] Z. Jin, T.M. Eikevik, P. Nekså, A. Hafner, R. Wang, Annual energy performance of R744 and R410A heat pumping systems, Applied Thermal Engineering 117 (2017) 568–576, https://doi.org/10.1016/j.applthermaleng.2017.02.072.

[19] T.R. Khamma, Y. Zhang, S. Guerrier, M. Boubekri, Generalized additive models: An efficient method for short-term energy prediction in office buildings, Energy 213 (2020), 118834, https://doi.org/10.1016/j.energy.2020.118834.

[20] M. Magni, F. Ochs, S. de Vries, A. Maccarini, F. Sigg, Detailed cross-comparison of building energy simulation tools results using a reference office building as a case study, Energy and Buildings 250 (2021), 111260, https://doi.org/10.1016/j.enbuild.2021.111260.

[21] D.B. Crawley, L.K. Lawrie, F.C. Winkelmann, W.F. Buhl, Y.J. Huang, C.O. Pedersen, R.K. Strand, R.J. Liesen, D.E. Fisher, M.J. Witte, J. Glazer, EnergyPlus: creating a new-generation building energy simulation program, Energy and buildings 33 (4) (2001) 319–331, https://doi.org/10.1016/S0378-7788(00)00114-6.

[22] W.A. Beckman, L. Broman, A. Fiksel, S.A. Klein, E. Lindberg, M. Schuler, J. Thornton, TRNSYS The most complete solar energy system modeling and simulation software, Renewable energy 5 (1–4) (1994) 486–488, https://doi.org/10.1016/0960-1481(94)90420-0.

[23] T. Kalamees, IDA ICE: the simulation tool for making the whole building energy and HAM analysis, Annex 41 (2004) 12–21.

[24] Brück, D., Elmqvist, H., Mattsson, S.E. and Olsson, H., 2002, March. Dymola for multi-engineering modeling and simulation. In *Proceedings of modelica* (Vol. 2002). Citeseer.

[25] T. Zakula, M. Bagaric, N. Ferdelji, B. Milovanovic, S. Mudrinic, K. Ritosa, Comparison of dynamic simulations and the ISO 52016 standard for the assessment of building energy performance, Applied Energy 254 (2019), 113553, https://doi.org/10.1016/j.apenergy.2019.113553.

[26] https://modelica.org/modelicalanguage.html (Last access- 18-06-2022).

[27] M. Wetter, K. Benne, A. Gautier, T.S. Nouidui, A. Ramle, A. Roth, H. Tummescheit, S. Mentzer, C. Winther, Lifting the garage door on Spawn, an open-source BEM-controls engine, In the proceedings of the Building Performance Modeling Conference US (2021) 508–525.

[28] Wetter, M., Benne, K. and Ravache, B., 2021, September. Software Architecture and Implementation of Modelica Buildings Library Coupling for Spawn of EnergyPlus. In Proceedings of the 14th *Modelica Conference*, Linköping, Sweden,325-334. https://doi.org/10.3384/ecp21181325.

[29] https://www.energy.gov/eere/buildings/commercial-reference-buildings (Last access- 18-06-2022).

[30] MSL Modelica Standards library https://github.com/modelica/ModelicaStandardLibrary (Last access- 18-06-2022).

[31] TLK-Thermo GmbH, 2020a. TIL Suite – Simulates thermal systems, https://www.tlk-thermo.com/index.php/en/software/38-til-suite. (Last access- 18-06-2022).

[32] MBL Modelica Buildings Library https://simulationresearch.lbl.gov/modelica/ (Last access- 18-06-2022).

[33] S. Smitt, I. Tolstorebrov, A. Hafner, Performance improvement of integrated CO_2 systems with HVAC and hot water for hotels, Thermal Science and Engineering Progress 23 (2021), 100869, https://doi.org/10.1016/j.tsep.2021.100869.

[34] BITZER compressor manufacturer: https://www.bitzer.de/gb/en/ (Last access- 18-06-2022).

[35] American Society of Heating, Refrigerating and Air-Conditioning Engineers – ASHRAE 55:2004: Thermal Environmental Conditions for Human Occupancy ASHRAE, N.E. Atlanta, GA, US (2004).

[36] J. Laue, ASHRAE 62.1: using the ventilation rate procedure, Consult. Spec. Eng 55 (2018) 14–17.

[37] https://fmi-standard.org/ (Last access- 18-06-2022).

[38] Spawn of Energy Plus output variables list: https://build.openmodelica.org/Documentation/Buildings.ThermalZones.EnergyPlus.OutputVariable.html (Last access- 18-06-2022).

[39] https://github.com/NREL/EnergyPlus/blob/develop/testfiles/RefBldgSmallOfficeNew2004_Chicago.idf (Last access- 18-06-2022).

[40] L. Yang, H. Li, S.W. Cai, L.L. Shao, C.L. Zhang, Minimizing COP loss from optimal high-pressure correlation for transcritical CO2 cycle, Applied Thermal Engineering 89 (2015) 656–662, https://doi.org/10.1016/j.applthermaleng.2015.06.023.

[41] S.M. Liao, T.S. Zhao, A. Jakobsen, A correlation of optimal heat rejection pressures in transcritical carbon dioxide cycles, Applied Thermal Engineering 20 (9) (2000) 831–841, https://doi.org/10.1016/S1359-4311(99)00070-8.

[42] Wetter, M., Nouidui, T.S., Lorenzetti, D., Lee, E.A. and Roth, A., 2015, November. Prototyping the next generation energyplus simulation engine. In*Proceedings of the 3rd IBPSA Conference, Jeju island, South Korea*, 27-29.

[43] SPAWN: A software package for performing co-simulation involving EnergyPlus and Modelica: https://github.com/NREL/Spawn (Last access- 18-06-2022).

[44] Elarga, H and Hafner A., CO2heat pump/chiller system for a hotel in a tropical climate: a numerical investigation. In*Proceedings of the 15th IIR Gustav Lorentzen Natural Working Fluids Conference, 13th-15th June: ID: 0261.* https://doi.org/10.18462/iir.gl2022.0261.

[45] INDEE+ project: https://www.ntnu.edu/indee/indee (Last access- 18-06-2022).